Europace (2014) **16**, 405–415
doi:10.1093/europace/eut405

Multiscale computational analysis of the bioelectric consequences of myocardial ischaemia and infarction

Jose M. Ferrero*, Beatriz Trenor, and Lucia Romero

Departamento de Ingeniería Electrónica, Instituto I3BH, Universitat Politècnica de València, Camino de Vera s/n, 46022 Valencia, Spain

Received 30 May 2013; accepted after revision 21 November 2013

Ischaemic heart disease is considered as the single most frequent cause of death, provoking more than 7 000 000 deaths every year worldwide. A high percentage of patients experience sudden cardiac death, caused in most cases by tachyarrhythmic mechanisms associated to myocardial ischaemia and infarction. These diseases are difficult to study using solely experimental means due to their complex dynamics and unstable nature. In the past decades, integrative computational simulation techniques have become a powerful tool to complement experimental and clinical research when trying to elucidate the intimate mechanisms of ischaemic electrophysiological processes and to aid the clinician in the improvement and optimization of therapeutic procedures. The purpose of this paper is to briefly review some of the multiscale computational models of myocardial ischaemia and infarction developed in the past 20 years, ranging from the cellular level to whole-heart simulations.

Keywords Ischaemia • Infarction • Computer simulations • Mathematical models • Reentrant arrhythmias

Introduction

Ischaemia and infarction

Ischaemic heart disease is considered as the single most frequent cause of death, provoking more than 7 000 000 deaths every year worldwide.[1,2] A high percentage of patients suffering ischaemic heart disease experience sudden cardiac death,[3] with over to 450 000 cases being reported in the USA annually.[4] Almost 70% of them were probably caused by tachyarrhythmias associated to myocardial ischaemia.[4,5] It is therefore not surprising that an enormous body of research is being devoted to investigate the mechanisms underlying the relationship between myocardial ischaemia/infarction and arrhythmias.

Myocardial ischaemia usually results from the occlusion of a coronary artery, and can be defined as a condition in which the blood supply to heart cells is insufficient to meet their metabolic demands.[6] During the first 15 min after coronary artery occlusion ('phase 1A ischaemia'), the heart suffers profound metabolic and electrophysiological changes at different scales. At the subcellular level, electrolyte concentrations change, adenosine triphosphate (ATP) and oxygen levels decline, and pH decreases.[7] At the cellular level, ion channel activity changes, resting potential becomes less negative, action potential duration (APD) shortens, upstroke velocity decreases, and cells loose excitability.[7] At the organ level, conduction velocity (CV) decreases and severe tachyarrhythmias may easily develop.[8,9] During the period that follows ('phase 1B ischaemia', 15–45 min post-occlusion), cellular uncoupling develops,[10] ischaemic tissue becomes inexcitable, and arrhythmias may re-appear after a safe period of several minutes.[11,12]

When the acute phase terminates, the infarcted tissue begins to heal[13] (subacute phase of myocardial infarction, MI) and spontaneous ventricular arrhythmias can take place in this period.[14,15] Finally, complete healing and scar formation occurs after several days (or weeks). In this chronic phase of MI, reentrant ventricular tachycardias (VTs) are still inducible, indicating that the arrhythmogenic substrate is still present, *albeit* the mechanisms of these chronic-phase arrhythmias are different from those of the acute phase.

Simulation of ischaemia and infarction

In the past decades, integrative computational simulation has become a powerful tool to complement experimental and clinical research when trying to elucidate the intimate mechanisms of ischaemic electrophysiological processes.[16–22] The heart is a particularly appropriate organ to be computationally simulated on a multiscale basis because of the long history of cardiac cell modelling[23] and the continuous interaction between experiments and simulation. From the

* Corresponding author. Tel: +34 96 3877007 (ext. 67037), Email: cferrero@gbio.i3bh.es

earliest Luo–Rudy[24] models for guinea-pig ventricular cells to the most recent electrophysiological model of human ventricular myocytes,[25] it has become possible to dynamically compute ionic currents through sarcolemmal channels and transporters, ion concentrations (including Ca^{2+} levels in the different subcellular compartments), and action potentials (APs) with great degree of electrophysiological detail. In parallel, medical imaging techniques have enabled us to reconstruct heart anatomy and structure '*in silico*', allowing multiscale computational simulations in which genetic defects, for instance, can be linked to the whole organ behaviour. These 'virtual hearts' are today a perfect example of how an integrative biology approach may aid in the understanding of cardiac arrhythmias and in the improvement of therapeutic techniques such as drug administration, electrical defibrillation, or radiofrequency ablation.

Acute myocardial ischaemia and MI are among the most successfully simulated cardiac pathologies.[17] Experimental understanding of the intimate mechanisms of acute ischaemia is particularly difficult due to the complex dynamics and unstable nature of the phenomenon, and the fact that most lethal arrhythmias occur before hospital admission makes it almost impossible to carry out systematic clinical studies. Also, the potential immediacy of death associated to ischaemic arrhythmias poses insurmountable ethical and practical obstacles. Therefore, computer simulations are of special importance. In the subacute and chronic stages of MI, simulations are also of great interest to aid the clinician during ablation interventions. This therapeutic procedure has unsatisfactory rates ranging from 50 to 90%, and a consensus on the optimum approach does not exist.[26] Thus, multiscale image-based simulation is becoming a powerful tool which can provide guidance in defining the optimum ablation strategy.

Outline

The purpose of this paper is to briefly review some of the multiscale computational models of myocardial ischaemia and MI developed in the past 20 years. The review begins with a discussion of different models of acute ischaemia at the cellular level and then deals with the modelling of ischaemia-related tissue heterogeneities [i.e. the ischaemic border zone (BZ)]. Then, simulations of the electrical consequences of regional ischaemia (in the form of increased reentrant-type arrhythmia vulnerability) are discussed, both in Phases 1A and 1B ischaemia. Next, models for the electrical and structural remodelling of infarcted tissue are presented. Finally, simulation of the electrical activity in chronically infarcted tissue is discussed, including a very novel approach to myocardial ablation which uses image-based electrical simulations.

Simulation of ischaemia at the cellular level

It has been known for many years that acute ischaemia has three major components that result from cessation of blood flow: acidosis, hypoxia, and hyperkalaemia.[27,28] Intracellular and extracellular pH values can drop from 7.2–7.4 to 6.2–6.4 in the first 10–20 min of ischaemia.[29] Oxygen deprivation provokes a moderate decline in ATP levels and an increase in adenosine diphosphate (ADP) concentration in the intracellular medium.[30] Extracellular K^+ concentration ($[K^+]_o$) can increase more than two-fold in the first 10–15 min post-occlusion before plateauing for another 15–20 min.[31–34] Each of these phenomena affects ion channels (and thereby APs) in a different manner[35] and ultimately set the stage for reentrant activity.[7]

Simulating acidosis in Phase 1A ischaemia

In almost all ischaemic cellular models, the effects of acidosis are mimicked by reducing the maximum conductance of the fast Na^+ channels and the L-type Ca^{2+} channels.[36–38] A direct consequence of these changes is a reduction in cell excitability and upstroke velocity.[39,40] Very recently, Roberts and Christini included the Na^+/H^+ and other exchangers in the Luo–Rudy model[41] to analyse reperfusion arrhythmogenesis,[42] creating a new model which can accurately reproduce acidosis in acute ischaemia.

Simulating hypoxia in Phase 1A ischaemia

Simulation of the electrophysiological effects of hypoxia has historically deserved much attention. The decline in ATP level reduces Na^+/K^+ pump (I_{NaK}) activity and activates the ATP-sensitive K^+ current ($I_{K(ATP)}$),[43] which is almost dormant in normoxic myocardium. To assess the electrophysiological effects of $I_{K(ATP)}$ activation, Ferrero *et al.*[44] proposed a model for $I_{K(ATP)}$ which included the modulation exerted by ATP and ADP,[30] intracellular Mg^{2+} and Na^+,[45] and $[K^+]_o$.[45] This model was incorporated into the Luo–Rudy ionic model[24,45] and APs were simulated under hypoxic conditions to try to elucidate the role of $I_{K(ATP)}$ activation in the well-known APD shortening in acute ischaemia.[46] The main results of the simulations, depicted in *Figure 1A*, showed that opening of very few (<1%) K_{ATP} channels may provoke a strong shortening in APD, with activation of only 0.6% of K_{ATP} channels needed to account for a 50% reduction in APD. These results confirmed the validity of the 'spare channel hypothesis'[48] in the heart, something which was not completely clear in view of some experimental results.[49] According to the results by Ferrero *et al.*, hyperkalaemia was only a secondary factor in explaining APD shortening during Phase 1A ischaemia. Using a similar model for $I_{K(ATP)}$, Shaw and Rudy[39,50] arrived to analogous results.

Recently, a new and more comprehensive model for $I_{K(ATP)}$ was developed. Using new experimental data on Mg^{2+}, ATP, and MgADP regulation of K_{ATP} channels and on the channel structure, Michailova *et al.*[51] reformulated the current and incorporated it to an ionic-metabolic model appropriate for excitation–metabolic coupling simulations under ischaemic conditions in the transmural ventricular wall.[52] The model was used to predict that K_{ATP} channels are activated transmurally with the smallest reduction in ATP in epicardial cells and largest in endocardial cells during Phase 1A ischaemia and that inhomogeneous accumulation of metabolites in the transmural ventricular tissue may alter K_{ATP} channel opening in a very irregular manner, causing differential APD shortening across the ventricular wall.[52]

Simulating hyperkalaemia in Phase 1A ischaemia

The causes and effects of hyperkalaemia have also deserved attention in computational simulation. Ischaemic elevation of $[K^+]_o$ forces

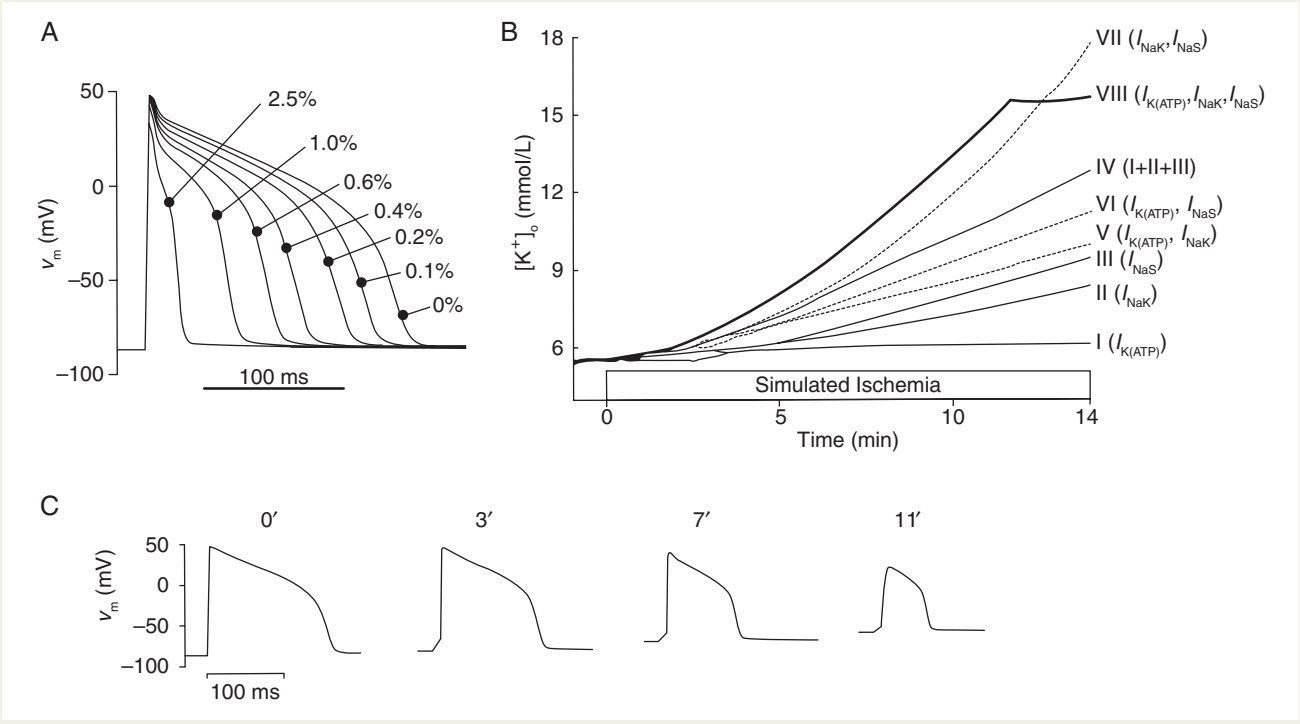

Figure 1 Simulation of Phase 1A ischaemia at the cellular level. (*A*) Hypoxic APs for different activation degrees of ATP-sensitive K^+ channels. Numbers indicate percentage of open channels. Reproduced from Ferrero *et al.*[44] with permission. (*B*) Timecourse of extracellular K^+ concentration during acute ischaemia. Each trace corresponds to a different ionic event: progressive activation of ATP-sensitive K^+ channels ($I_{K(ATP)}$, Trace I), inhibition of the Na^+/K^+ pump (I_{NaK}, Trace II), activation of an ischaemic slow-activated inward Na^+ current (I_{NaS}, Trace III), algebraic sum of the three traces (Trace IV), combinations of two mechanisms (Traces V–VII), and combination of the three mechanisms (Trace VIII). (*C*) Action potentials from isolated ventricular myocytes at different minutes post-occlusion. Panels (*B*) and (*C*) modified from Rodriguez *et al.*[47] with permission.

cellular resting potential to become less negative (diastolic depolarization) and thus reduces cell excitability and delays its recovery (inducing post-repolarization refractoriness, PRR).[53] These effects of hyperkalaemia have been reproduced by simulating APs of single myocytes subject to acutely ischaemic conditions in isolated myocytes[39] and one-dimensional (1D) strands.[50] Although these changes in cell excitability are strongly pro-arrhythmic because they promote unidirectional block (UDB) and reentry,[8,9,54,55] the intimate causes of cellular K^+ loss are still not well understood.

In 2002, Rodriguez *et al.*[47] used a single-cell model which dynamically calculated ion transfer and fluxes between three compartments (intracellular, interstitial cleft, and bulk extracellular media) in ischaemic conditions. To simulate ionic currents and APs, the model used the Luo-Rudy membrane kinetics[24,56] including the formulation of $I_{K(ATP)}$ by Ferrero *et al.*[44] and an ischaemia-activated slow Na^+ current (I_{NaS}).[57] *Figure 1B* depicts the main results obtained with the model. According to the simulations, the concurrence of three mechanisms is needed to explain the biphasic timecourse of $[K^+]_o$ in Phase 1A ischaemia, namely $I_{K(ATP)}$ current activation,[58] I_{NaK} partial inhibition,[59] and I_{NaS} activation.[57,58,60] The participation of only one or two of these mechanisms cannot explain the experimentally observed $[K^+]_o$ increase neither quantitatively nor qualitatively. Due to the non-linear nature of the phenomenon, the algebraic addition of the separate effects of the three mechanisms (Trace IV in *Figure 1B*) does not reproduce the timecourse of $[K^+]_o$ either. However, if the three mechanisms take place simultaneously, the non-linear interactions between them increases the rate of $[K^+]_o$ rise, generates a plateau, and the biphasic increase of $[K^+]_o$ can be nicely reproduced (Trace VIII in *Figure 1B*). Interestingly, the quantitative contribution of $I_{K(ATP)}$ to the rise in $[K^+]_o$ is almost negligible (Trace I), but its participation is essential to generate the plateau in $[K^+]_o$ (compare Traces VII and VIII). The simulations also show that K^+ efflux mainly takes place through the time-independent K^+ channels (I_{K1}). Although these findings are difficult to be obtained using solely experimental means, further experiments should be undertaken to confirm the hypothesis suggested by the model.

Incorporating the effects of acidosis, hypoxia, and hyperkalaemia into an AP model, the electrical activity of the Phase 1A ischaemic cell can be computed and explained.[39,50] *Figure 1C* shows simulated APs of an isolated myocyte during four different stages of Phase 1A ischaemia (0, 3, 7, and 11 min post-occlusion, respectively).[47] The changes observed in APs are consistent with the experimental findings.[30,32,35,61]

Simulating Phase 1B ischaemia

To simulate Phase 1B ischaemia, Pollard[62] proposed additional modifications in ionic currents and intracellular Ca^{2+} handling, including the acidotic inhibition of the Na^+/Ca^{2+} exchanger, an enhancement of the background Ca^{2+} current and the non-selective Ca^{2+}-sensitive cation current, and a reduction in the sarcoplasmic

reticulum Ca^{2+} release current and the sarco/endoplasmic reticulum Ca^{2+}-ATPase pump.

The border zone in acute ischaemia

Modelling border zone gradients

In most cases, ischaemia is caused by the occlusion of a coronary artery and thus its nature is regional. A central ischaemic zone (CIZ) is formed, constituted by cells directly affected by the lack of blood flow, while cells away from the CIZ are unaltered and form the normal zone (NZ). The transition between both zones is not abrupt but instead an ischaemic BZ develops in which a gradient of ion and metabolite concentrations exists. This high degree of heterogeneity sets the stage for reentry.[55,63] The width of the BZ for each species is variable and has been characterized experimentally for some ions (particularly K^+),[64–67] but the profile and extension of the BZ for other species remains unclear.

Potse *et al.*[68] used a 1D diffusive model for K^+ ions to establish the spatial profile of $[K^+]_o$ across the BZ. The results predict a non-linear $[K^+]_o$ spatial evolution within the BZ, showing a steep rise in the BZ adjacent to the NZ and a more flattened behaviour near the CIZ. The authors demonstrate that the diffusion constant, which would be needed to explain the experimentally observed profile of K^+ in the BZ is too large, suggesting that physical diffusion is not the only mechanism that plays a role in the establishment of the BZ. Pulsative flow in the arterial and venous bed could be the other mechanisms involved.[66]

More recently, Niederer[69] extended the model to other species (Na^+, Ca^{2+}, Cl^- and H^+, among others). An experimental measurement of the gradients of these ions in ischaemia is hampered by low spatial and/or temporal resolutions.[66,70] The model developed by Niederer is extremely comprehensive, as it includes dynamic descriptions of membrane kinetics, ionic currents, diffusive ion fluxes, and Ca^{2+} regulation. The author was able to simulate the spatiotemporal profile of intracellular and extracellular concentrations. The results show that the ischaemic BZ is larger for extracellular K^+ (four times wider than the Na^+ BZ, for instance), which can be explained by the voltage-dependent nature of K^+ channels, and also that intracellular and extracellular K^+ concentrations may decrease within the CIZ due to electrogenic drift.

Simulating electrical activity in regional ischaemia

When the NZ, BZ, and CIZ are included in a tissue model coupled to an ischaemic AP model, the electrical activity of an acutely ischaemic tissue can be simulated. Ferrero *et al.*[71] conducted simulations in an electrophysiologically detailed 2D anisotropic tissue subject to 10 min of ischaemia. The tissue comprised a circular CIZ surrounded by a ring-shaped BZ with a width of 1 cm for $[K^+]_o$ and pH[64,66,72] and 1 mm for ATP/ADP,[72] enclosed in normal tissue (NZ). The results, shown in *Figure 2*, reveal profound electrophysiological changes within the BZ under normal pacing. First, CV slightly increases when entering the BZ (due to 'supernormal conduction'),[50] but decreases in the second half of the BZ, plateauing at approximately one-third of its normal value in the CIZ due to the combined effects of hyperkalaemia and acidosis (see *Figure 2A*). Secondly, a sharp reduction in APD and effective refractory period (ERP) is found in the normal side of the BZ (due to abrupt $I_{K(ATP)}$ activation

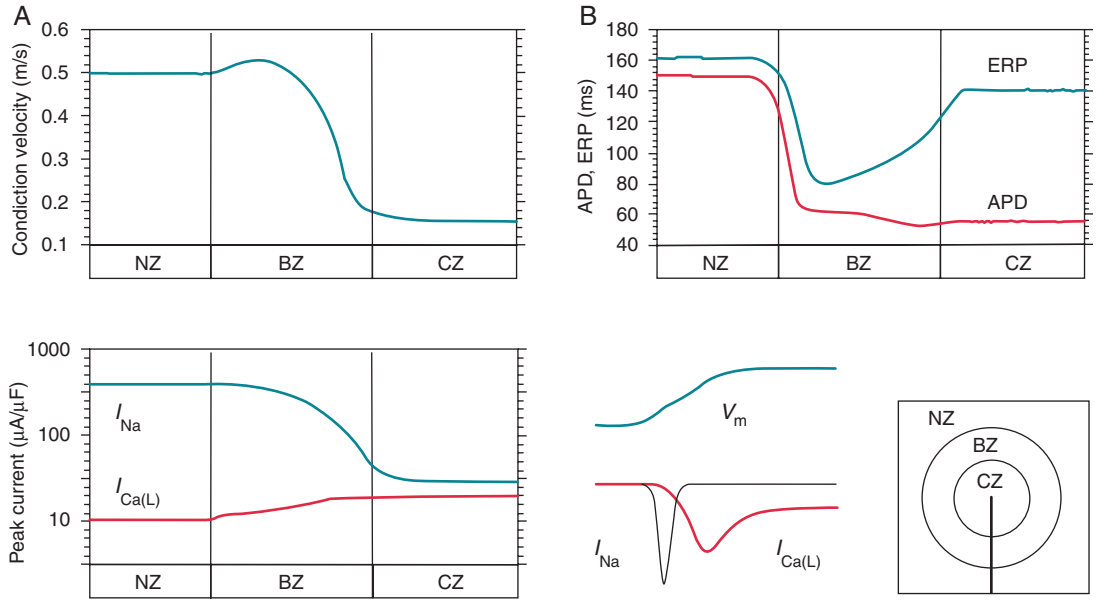

Figure 2 Simulation of regional Phase 1A ischaemia in a 2D tissue. (*A*) Longitudinal conduction velocity in the NZ, BZ, and central zone (CZ) along the vertical strand depicted in panel (*E*). (*B*) Effective refractory period (ERP) and APD. (*C*) Peak Na^+ and L-type Ca^{2+} currents (I_{Na}, $I_{Ca(L)}$). (*D*) Time-courses of transmembrane potential (V_m), I_{Na}, and $I_{Ca(L)}$ in the centre cell. (*E*) Schematic of the tissue. Reproduced from Ferrero *et al.*,[71] © 2003 World Scientific Publishing Company with permission.

in the first millimetre of the BZ), but ERP subsequently increases across the BZ reaching almost normal values in the CIZ, mainly due to hyperkalaemia (*Figure 2B*). Thus, the model predicts a strong gradient in ERP across the BZ and a high degree of PRR (>80 ms) in the CIZ, which is consistent with experimental findings by Zaitsev *et al.*[63] in regionally ischaemic pig hearts. Thirdly, as shown in *Figure 2C*, acidosis and hyperkalaemia strongly reduce the inward Na^+ current (I_{Na}) peak in the CIZ, reaching a value comparable with the L-type Ca^{2+} current ($I_{Ca(L)}$) peak. This can be further appreciated in *Figure 2D*, where the timecourse of AP, I_{Na}, and $I_{Ca(L)}$ during the depolarization and early plateau phases is shown. The upstroke of the AP is divided into two distinct components (one supported by I_{Na} and the other by $I_{Ca(L)}$), something which has been observed experimentally.[7,53,73,74] The enhanced role of $I_{Ca(L)}$ in ischaemic propagation favours conduction block and the appearance of alternans, which in turn may provoke reentry as demonstrated also by Shaw and Rudy[40] and Bernus *et al.*[75] This highly heterogeneous substrate favours reentrant arrhythmias.

When Phase 1B ischaemia is reached, the mid-myocardial part of the CIZ becomes inexcitable,[76] acting as a partially depolarized sink. Viable cell layers survive in the subepicardium and the subendocardium, with ischaemic damage increasing over time.[77] Cellular uncoupling between the inexcitable mid-myocardium and the survival layers begins to develop.[10] This substrate was modelled by Jie *et al.*[78,79] to study Phase 1B ischaemia arrhythmogenesis.

Vulnerability to reentry in ischaemia

Using the same tissue model for Phase 1A ischaemia described previously, Ferrero *et al.*[71] studied the inducibility of reentry. When paced at the same site as the basic beat, a premature stimulus could induce figure-of-eight reentrant patterns which nicely resembled those obtained experimentally.[8,9,55,80]

Similar reentrant patterns were obtained from simulations conducted in a 3D reconstruction of the human ventricles with realistic anatomy and structure [obtained from diffusion tensor magnetic resonance imaging (DT-MRI)] and transmural heterogeneity (with different ionic computational models for epicardial, endocardial, and mid-myocardial cells).[81] *Figure 3* shows the transmembrane potential distribution in selected instants just after the delivery of a premature stimulus in the subendocardial BZ, where premature excitations (the trigger for arrhythmia induction) normally originate.[8,35,66,74] An arc of functional conduction block develops in the innermost side of the BZ (third snapshot), caused by the prolonged refractoriness of

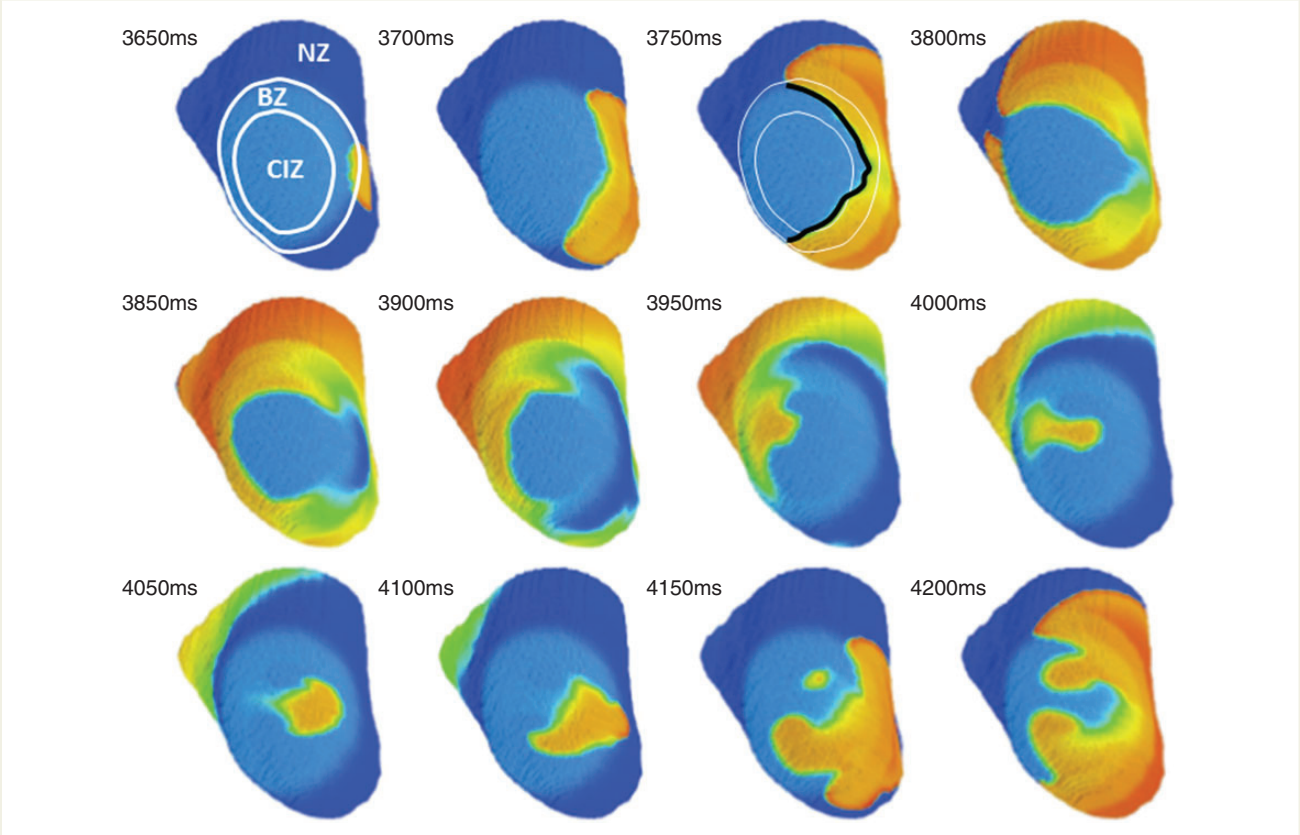

Figure 3 Simulation of Phase 1A ischaemia at the organ level. Panels show voltage snapshots (colour-coded membrane voltage) corresponding to the anterior epicardial wall at 12 different instants after the delivery of a premature stimulus. The approximate location of the NZ, BZ, and CIZ is shown in the first panel. The black line in the third panel shows an arc of block.

the tissue (PRR is near its maximum at that site), giving rise to UDB and figure-of-eight reentry.[82]

The timecourse of arrhythmia vulnerability

According to different experimental and clinical observations, the likelihood of arrhythmic events reaches a maximum before the 10th minute, decreases again giving rise to an arrhythmias-scarce period at the end of Phase 1A, and increases subsequently in Phase 1B.[11,12,83] The reasons for this triphasic behaviour are still not completely established. Using the same 2D model described above, Trenor *et al.*[84] studied the time-evolution of reentry inducibility during the first 10 min of ischaemia. The authors quantified the 'vulnerable window' (VW, defined as the time interval during which a premature stimulus—delivered after a conditioning stimulus—triggers reentry) at selected time points post-occlusion. The results were consistent with experimental observations: the VW begins to increase 6.5 min after the onset of ischaemia, peaks at the eighth minute and vanishes in the ninth minute. According to the simulation results, reentry needs the combination of severe hyperkalaemia with moderate hypoxia and acidosis to occur, and those conditions are met in the third-quarter (minutes 5–7.5) of Phase 1A ischaemia. Severe hyperkalaemia ($[K^+]_o > 12$ mmol/L) is needed to generate enough PRR to create an arc of block, while strong acidosis (weak I_{Na} and $I_{Ca(L)}$) and/or hypoxia (strong $I_{K(ATP)}$) would in turn block retrograde propagation in the CIZ creating a bidirectional block that prevents reentry.[84]

By using the same AP and tissue and model, the same group conducted simulations to assess the pro-arrhythmic or antiarrhythmic effects of two well-known drugs. According to their simulation results, pinacidil[85] was shown to be pro-arrhythmic (incrementing the VW) at low concentrations but protective at concentrations >10 μmol/L,[86] while lidocaine[87] facilitates the onset of reentry in ischaemic ventricular tissue.[88]

In a similar study using a 2D slice of virtual acutely ischaemic ventricular tissue, Tice *et al.* highlighted the importance of transmural heterogeneity in the development of Phase 1A arrhythmias.[89] Experimental studies usually focus on epicardial manifestations of arrhythmias due to logical limitations related to the penetration depth of optical mapping techniques. In their simulation study, three BZs (lateral, endocardial, and epicardial) of different widths were defined, and transmural heterogeneities in the ischaemic severity were included (with $[K^+]_o$ rising at a faster rate in the subendocardium and hypoxia affecting more severely in the subepicardium). Their results suggest that transmural gradients of $I_{K(ATP)}$ activation strongly increase arrhythmogenesis, with almost no sustained reentrant activity observed in the absence of $I_{K(ATP)}$ heterogeneity. Reentrant likelihood also peaked in the eighth minute post-occlusion. The importance of transmural ischaemic heterogeneity was also stressed in the work by Weiss *et al.*[90] which used a 3D model of the human ventricles.

Dispersion of refractoriness and arrhythmia vulnerability

According to different experimental[63,67,91] and theoretical[92,93] studies, spatial dispersion of repolarization and/or refractoriness increases reentry vulnerability. Romero *et al.*[94] used a 2D ventricular model developed by Ferrero *et al.*[71,84] to test this hypothesis in the case of Phase 1A ischaemia. According to their results, summarized in *Figure 4*, ERP dispersion and arrhythmia vulnerability only correlate well in the first 8 min of ischaemia but diverge in the last part of Phase 1A, when arrhythmias cease to occur but ERP dispersion keeps increasing. According to their results, UDB took place in cells completely recovered from refractoriness in almost 50% of reentries. The authors argue that local source–sink relationship determines the formation of UDB, and propose a modified version of the safety factor (which quantifies the sink–source mismatch in the propagation process)[95,96] as a better tool to analyse the causes of UDB in ischaemia.

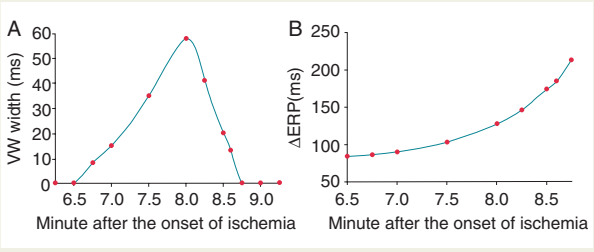

Figure 4 Timecourse of the VW duration (*A*) and dispersion of effective refractory period (ΔERP, *B*) during the first 10 min of ischaemia. Reproduced from Romero *et al.*[94] with permission.

The role of mechanoelectrical feedback

In all the simulations mentioned above, the trigger for reentry was artificially applied in the form of a premature stimulus externally delivered at a certain site (normally the subendocardial BZ),[8,66,74] so no inference can be made about the originating mechanism of reentry. Recent multiscale simulations by Jie *et al.*[97] suggest that mechanoelectrical feedback may play a pivotal role. The simulations involved 3D anatomically and structurally accurate virtual rabbit ventricles in which occlusion of the LAD artery was simulated. The ionic model employed included a mathematical description of two distinct mechanosensitive channels,[98] and it also included a novel bidomain electromechanical model. According to their results, mechanosensitive ionic channels[99] are recruited due to the non-uniformity of mechanical strain during acutely ischaemic contractions, resulting in suprathreshold depolarizations in the BZ which act as the trigger of the premature beat that, in turn, elicits reentry. In addition, delayed after-depolarizations (DAD) also resulting from mechanoelectrical feedback in the ischaemic region can contribute to lower excitability, enhancing refractoriness in the CIZ and favouring reentry.

Arrhythmias in Phase 1B ischaemia

Less attention has been paid to the mechanisms of arrhythmias in Phase 1B ischaemia. In 2003, Pollard *et al.*[100] conducted simulations in a 1D strand comprising 1 cm of normal tissue coupled to 1 cm of cells affected by Phase 1B ischaemia. The results indicated that suprathreshold DADs develop in the ischaemic zone and only propagate to normal tissue in the form of APs when intermediate uncoupling between the two zones is present. The fact that moderate

uncoupling is an important contributor to Phase 1B arrhythmogenesis was further stressed by the work of Jie *et al.*,[78] in which they coupled an inexcitable mid-myocardial zone to a surviving subepicardial layer via a thin coupling layer. The results suggested that heterogeneous uncoupling between layers enhance ERP dispersion in the subepicardium, thus increasing reentry vulnerability. Complete uncoupling eliminated arrhythmias. In a more recent work, Jie and Trayanova[79] improved the model by using 3D rabbit ventricle geometry and simulating a more complex substrate structure which comprised a CIZ with inexcitable mid-myocardium and surviving subepicardial and subendocardial layers, as well as lateral BZs. According to their results, the degree of hyperkalaemia in the subepicardium was key, as it led to the induction of reentrant activity. Vulnerability to reentry was biphasic, with increased cellular uncoupling and reduction of the width of the lateral BZ increasing reentry inducibility.

Simulating global ischaemia

When ischaemia results from a coronary artery occlusion, it is regional by nature, but during ventricular fibrillation (VF) ischaemia becomes global as perfusion of the myocardium is interrupted. However, simulation works dealing with global ischaemia are not as abundant as those that model regional ischaemia. Among them, a recent paper[101] simulates global ischaemia in a 2D virtual tissue to provide some insights into the effects of ischaemia on the organization of VF. With a different aim, Rodriguez *et al.*[103] simulated global ischaemia in a 2D slice of myocardium[102] and in 3D rabbit ventricles to study the effects of Phase 1A global ischaemia on the upper limit of vulnerability to electric shocks in the context of electrical defibrillation.

Electrical and structural remodelling in infarcted tissue

Three to five days after the initial ischaemic event, electrical[13,14] and structural[13] remodelling of the epicardial BZ (EBZ) begins. These changes in the substrate can eventually generate arrhythmias in the subacute and chronic phases of MI[104] and have received attention in the past 10 years from the computational simulation community.

Electrical remodelling

Within the EBZ, experimental studies have recorded shorter,[13] similar,[13,105] or longer[106] APD than in normal myocardium. However, the EBZ has a longer refractory period due to the existence of PRR.[14,107] Using experimental data from remodelled ionic currents, Cabo and Boyden[108] formulated a computational model for EBZ cells. They modified the Luo–Rudy model to include alterations in the maximal conductance and kinetics of I_{Na},[105] $I_{Ca(L)}$,[109] I_{Kr},[110] I_{Ks},[111] and I_{K1}.[111] More recently, Decker and Rudy[112] developed a new model of the remodelled EBZ by additionally altering the maximum conductance and kinetics of I_{to2}^{113} and I_{to1}.[105] Applying these modifications to the basic Luo–Rudy model, the authors were able to reproduce the aforementioned features of APs of cells in the EBZ. Even more recently, McDowell *et al.*[114] adapted a rabbit AP model in the same direction.

Structural remodelling

In reference to structural remodelling, gap junctional changes and fibrotic remodelling have been observed in post-infarcted hearts[111,112] with conduction disturbances observed in the healing infarct BZ being related to intercellular uncoupling.[115,116] Marked alterations in the organization of intercellular connections occur in the EBZ, leading to non-uniform conduction, fractionated electrograms, and reentry.[116] Several theoretical investigations using computer simulations have addressed the role of altered cellular coupling on AP conduction.[117,118] Cellular uncoupling not only decreases CV, but it may create a substrate that facilitates the propagation of ectopic activity.[119,120] It is thus an important factor to consider when implementing realistic electrical models of the infarcted heart in the subacute and chronic phases.

Experimental evidence exists according to which myofibroblasts proliferate following MI, especially in the peri-infarct zone.[121,122] Electrical coupling between myofibroblasts and myocytes is well established in cell culture[123] and the presence of fibrotic areas in the ventricle leads to altered and discontinuous conduction and fractionated electrograms.[124,125] Several theoretical studies focusing on the electrotonic coupling between fibroblasts and myocytes use computational models of the passive and active electrical behaviour of fibroblasts.[126–128] Simulations reveal significant electrophysiological consequences of coupling fibroblasts to myocytes at the cellular level, such as partial diastolic depolarization of the myocyte and significant shortening of its APD.[126] Also, the critical pacing cycle length at which alternans occur is changed by fibroblast–myocyte coupling.[129] In results obtained from 1D and 2D simulations, conduction disturbances arise in the presence of fibrosis[130,131] and changes in electrical restitution properties occur, leading to spiral wave instability.[132,133] Using 2D simulations, Xie *et al.*[129] observed an increased vulnerability to reentry in the presence of fibrosis. Fractionated electrograms were also obtained in 2D-simulated ventricular tissues with different fibrosis densities.[134]

Simulation of myocardial infarction at the organ level

Three-dimensional ventricular simulations including fibrosis are very recent. McDowell *et al.*[114] simulated the electrical activity of anatomically realistic rabbit ventricles in the presence of an infarction scar, a remodelled peri-infarct zone and different levels of fibrosis. The authors observed an increase in the vulnerability to reentry in the presence of intermediate fibrosis, while high densities of fibroblasts reduced the probability of reentry. To run the simulations, they developed a 3D computational model of the chronically infarcted rabbit ventricles based on the MRI. Recent advances in the MRI technologies have facilitated the imaging of geometry and tissue architecture at improved resolution, so image-based methods have been recently developed to construct computational models,[135] and many of them focus on the arrhythmogenic behaviour of the infarcted heart.

Rantner *et al.*[136] analysed the mechanisms of decreased defibrillation efficacy in infarcted hearts using an improved model of the rabbit infarcted ventricle. Vigmond *et al.*[137] analysed reentrant mechanisms in a canine infarction 3D model also using image-based modelling techniques. Their model included a scar and the BZ with electrical

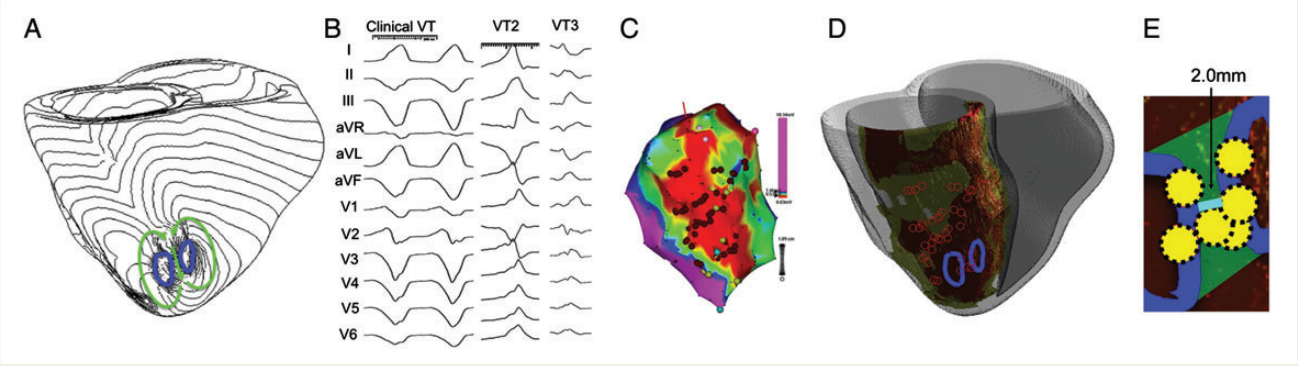

Figure 5 Comparison between image-based simulation of chronic MI and standard (non-simulation) approach. (*A*) Activation map of a simulation of VT. Arrows indicate wave propagation of reentrant circuits, and lines indicate arcs of block. (*B*) Twelve-lead electrocardiogram of inducible VTs from the standard approach. (*C*) Three-dimensional CARTO map with colour-coded voltages (purple: normal myocardium; blue, green, and yellow: infarct BZs; red: scar) from the standard approach. Circles represent ablation sites. (*D*) Pre-ablation MRI showing infarct geometry (orange: scar; yellow: heterogeneous zone; grey: non-infarcted myocardium). The lines of conduction block from the image-based simulation and the ablation sites from the standard approach are co-registered on the heart geometry. (*E*) Potential target region for ablation (green area) estimated from the image-based simulation. The shortest possible line of ablation that spans the target region is indicated in cyan. The ablation sites that fell within the estimated ablation target (green area) are indicated by yellow circles. Modified from Ashikaga *et al.*[141] with permission.

remodelling. Swine models of MI have also been reconstructed based on the MRI.[138–140] Pop *et al.*[138] showed that computer simulation based on *ex vivo* DT-MRI could predict the VT circuit obtained in swine electrophysiological studies. Their 3D model included healthy tissue, scar, and the BZ using a two-variable model of the AP. Similarly, Ng *et al.*[140] included electrically remodelled grey zones and infarct cores in swine hearts. Ventricular tachycardia was induced in different virtual models and showed that a combination of infarct scars and peri-infarct zones is needed for VT generation. Similar reentrant circuits were obtained in the electrophysiological studies and in the virtual ones, demonstrating that image-based modelling may be helpful when planning catheter ablation strategies. Indeed, very recently, Ashikaga *et al.*[141] tested the feasibility of image-based simulation to estimate ablation targets in human VT, highlighting the effectiveness of this non-invasive tool. As shown in *Figure 5*, their model includes infarct zones, grey zones with electrical remodelling, and healthy zones. When ablation in the human patient was done within the zone predicted by the model, successful termination of reentry was accomplished. This model is state-of-the-art in image-based simulation oriented to ablation strategy optimization.

Conclusions

This article provided a brief review of some of the multiscale computational models of myocardial ischaemia and MI developed in the past years. The models discussed here are examples of how computer simulations may help to understand the electrical consequences of ischaemia and MI and to improve treatments of subsequent cardiac arrhythmias. At the cellular level, simulations have contributed to elucidate the ionic mechanisms responsible for the ischaemia-induced changes in APs and ionic concentrations and have aided in better understanding how the ischaemic BZ is established. Regarding ischaemic arrhythmogenesis, the models have helped to clarify the role of acidosis, hypoxia, and hyperkalaemia in the onset and maintenance of ischaemic reentry and to theoretically explain the biphasic nature of arrhythmia vulnerability in Phase 1A ischaemia. Simulations have also shed new light on the role of dispersion of refractoriness, source–sink mismatch, and mechanoelectrical feedback in arrhythmogenesis.

Today, computational simulations are also helping to improve therapeutic techniques to stop and/or prevent arrhythmias in ischaemic patients. Modelling the interaction between different drugs (such as lidocaine or pinacidil) and their molecular targets has enabled us to explain (and, ideally, predict) the pro-arrhythmic or antiarrhythmic effects of these drugs in an ischaemic scenario. Also, recent works are beginning to show how computer simulations can be useful to improve electrical arrhythmia treatment.

In the task of integrating computer simulation techniques in daily clinical practice in the context of ischaemia and MI, important limitations are yet to be addressed. At the cellular level, ionic models need to be improved using new patch-clamp data from human ischaemic hearts. At the tissue level, it is still impossible to visualize the actual fibre orientation of the *in vivo* infarcted heart of a patient. When these and other limitations are overcome, the use of computational simulations to optimize myocardial ablation procedures in infarcted patients,[141] for instance, will become a real possibility.

Conflict of interest: none declared.

Funding

This work was partially supported by the 'VI Plan Nacional de Investigación Científica, Desarrollo e Innovación Tecnológica' from the Ministerio

de Economía y Competitividad of Spain (grant number TIN2012-37546-C03-01) and the European Commission (European Regional Development Funds—ERDF—FEDER), and by the Dirección General de Política Científica de la Generalitat Valenciana (grant number GV/2013/119).

References

1. Steg PG, James SK, Atar D, Badano LP, Blomstrom-Lundqvist C, Borger MA *et al.* ESC Guidelines for the management of acute myocardial infarction in patients presenting with ST-segment elevation. *Eur Heart J* 2012;**33**:2569–619.
2. Roger VL, Go AS, Lloyd-Jones DM, Benjamin EJ, Berry JD, Borden WB *et al.* Heart disease and stroke statistics—2012 update: a report from the American Heart Association. *Circulation* 2012;**125**:e2–220.
3. Zipes DP, Wellens HJ. Sudden cardiac death. *Circulation* 1998;**98**:2334–51.
4. Goldberger JJ, Cain ME, Hohnloser SH, Kadish AH, Knight BP, Lauer MS *et al.* American Heart Association/American College of Cardiology Foundation/Heart Rhythm Society scientific statement on noninvasive risk stratification techniques for identifying patients at risk for sudden cardiac death: a scientific statement from the American Heart Association Council on Clinical Cardiology Committee on Electrocardiography and Arrhythmias and Council on Epidemiology and Prevention. *Circulation* 2008;**118**:1497–518.
5. Rubart M, Zipes DP. Mechanisms of sudden cardiac death. *J Clin Invest* 2005;**115**:2305–15.
6. Ferrero JM, Ferrero A, Trenor B, Montilla F, Saiz J, Rodriguez B. Ischemia. In: Akay M (ed) *Wiley Encyclopedia of Biomedical Engineering*. Hoboken, NY, USA: John Wiley and Sons; 2006.
7. Wit AL, Janse MJ, Mount K (eds). Ventricular arrhythmias in the acute phase of myocardial ischemia and infarction. *The Ventricular Arrhythmias of Ischemia and Infarction: Electrophysiological Mechanisms*. Mount Kisko, NY, USA: Futura Publishing Co; 1993.
8. Janse MJ, van Capelle FJ, Morsink H, Kleber AG, Wilms-Schopman F, Cardinal R *et al.* Flow of 'injury' current and patterns of excitation during early ventricular arrhythmias in acute regional myocardial ischemia in isolated porcine and canine hearts. Evidence for two different arrhythmogenic mechanisms. *Circ Res* 1980;**47**:151–65.
9. Janse MJ, Kleber AG. Electrophysiological changes and ventricular arrhythmias in the early phase of regional myocardial ischemia. *Circ Res* 1981;**49**:1069–81.
10. de Groot JR, Wilms-Schopman FJ, Opthof T, Remme CA, Coronel R. Late ventricular arrhythmias during acute regional ischemia in the isolated blood perfused pig heart. Role of electrical cellular coupling. *Cardiovasc Res* 2001;**50**:362–72.
11. Kaplinsky E, Ogawa S, Balke CW, Dreifus LS. Two periods of early ventricular arrhythmia in the canine acute myocardial infarction model. *Circulation* 1979;**60**:397–403.
12. Smith WT, Fleet WF, Johnson TA, Engle CL, Cascio WE. The Ib phase of ventricular arrhythmias in ischemic in situ porcine heart is related to changes in cell-to-cell electrical coupling. Experimental Cardiology Group, University of North Carolina. *Circulation* 1995;**92**:3051–60.
13. Ursell PC, Gardner PI, Albala A, Fenoglio JJ Jr, Wit AL. Structural and electrophysiological changes in the epicardial border zone of canine myocardial infarcts during infarct healing. *Circ Res* 1985;**56**:436–51.
14. Lazzara R, Scherlag BJ. Electrophysiologic basis for arrhythmias in ischemic heart disease. *Am J Cardiol* 1984;**53**:1B–7B.
15. Pantridge JF, Webb SW, Adgey AA. Arrhythmias in the first hours of acute myocardial infarction. *Prog Cardiovasc Dis* 1981;**23**:265–78.
16. Noble D. Modeling the heart—from genes to cells to the whole organ. *Science* 2002;**295**:1678–82.
17. Rodriguez B, Trayanova N, Noble D. Modeling cardiac ischemia. *Ann N Y Acad Sci* 2006;**1080**:395–414.
18. Trayanova NA, Tice BM. Integrative computational models of cardiac arrhythmias—simulating the structurally realistic heart. *Drug Discov Today Dis Models* 2009;**6**:85–91.
19. Silva JR, Rudy Y. Multi-scale electrophysiology modeling: from atom to organ. *J Gen Physiol* 2010;**135**:575–81.
20. Trayanova NA. Whole-heart modeling: applications to cardiac electrophysiology and electromechanics. *Circ Res* 2011;**108**:113–28.
21. Trenor Gomis B, Romero L, Cardona K, Gomis-Tena J, Saiz J, Ferrero JM Jr. Multiscale modeling of myocardial electrical activity: from cell to organ. In: Gargiulo G (ed). *Applied Biomedical Engineering*. Rijeka: InTech 2011:337–60.
22. Trayanova NA, O'Hara T, Bayer JD, Boyle PM, McDowell KS, Constantino J *et al.* Computational cardiology: how computer simulations could be used to develop new therapies and advance existing ones. *Europace* 2012;**14**(Suppl 5):v82–9.
23. Noble D. Cardiac action and pacemaker potentials based on the Hodgkin-Huxley equations. *Nature* 1960;**188**:495–7.
24. Luo CH, Rudy Y. A dynamic model of the cardiac ventricular action potential. I. Simulations of ionic currents and concentration changes. *Circ Res* 1994;**74**:1071–96.
25. O'Hara T, Virag L, Varro A, Rudy Y. Simulation of the undiseased human cardiac ventricular action potential: model formulation and experimental validation. *PLoS Comput Biol* 2011;**7**:e1002061.
26. Aliot EM, Stevenson WG, Almendral-Garrote JM, Bogun F, Calkins CH, Delacretaz E *et al.* EHRA/HRS Expert Consensus on catheter ablation of ventricular arrhythmias: developed in a partnership with the European Heart Rhythm Association (EHRA), a Registered Branch of the European Society of Cardiology (ESC), and the Heart Rhythm Society (HRS); in collaboration with the American College of Cardiology (ACC) and the American Heart Association (AHA). *Europace* 2009;**11**:771–817.
27. Morena H, Janse MJ, Fiolet JW, Krieger WJ, Crijns H, Durrer D. Comparison of the effects of regional ischemia, hypoxia, hyperkalemia, and acidosis on intracellular and extracellular potentials and metabolism in the isolated porcine heart. *Circ Res* 1980;**46**:634–46.
28. Kodama I, Wilde A, Janse MJ, Durrer D, Yamada K. Combined effects of hypoxia, hyperkalemia and acidosis on membrane action potential and excitability of guinea-pig ventricular muscle. *J Mol Cell Cardiol* 1984;**16**:247–59.
29. Marban E, Kitakaze M, Koretsune Y, Yue DT, Chacko VP, Pike MM. Quantification of $[Ca2+]_i$ in perfused hearts. Critical evaluation of the 5F-BAPTA and nuclear magnetic resonance method as applied to the study of ischemia and reperfusion. *Circ Res* 1990;**66**:1255–67.
30. Weiss JN, Venkatesh N, Lamp ST. ATP-sensitive K^+ channels and cellular K^+ loss in hypoxic and ischaemic mammalian ventricle. *J Physiol* 1992;**447**:649–73.
31. Gasser RN, Vaughan-Jones RD. Mechanism of potassium efflux and action potential shortening during ischaemia in isolated mammalian cardiac muscle. *J Physiol* 1990;**431**:713–41.
32. Weiss J, Shine KI. $[K^+]_o$ accumulation and electrophysiological alterations during early myocardial ischemia. *Am J Physiol* 1982;**243**:H318–27.
33. Weiss J, Shine KI. Effects of heart rate on extracellular $[K^+]$ accumulation during myocardial ischemia. *Am J Physiol* 1986;**250**(Pt 2):H982–91.
34. Yan GX, Chen J, Yamada KA, Kleber AG, Corr PB. Contribution of shrinkage of extracellular space to extracellular K^+ accumulation in myocardial ischaemia of the rabbit. *J Physiol* 1996;**490**(Pt 1):215–28.
35. Carmeliet E. Cardiac ionic currents and acute ischemia: from channels to arrhythmias. *Physiol Rev* 1999;**79**:917–1017.
36. Kagiyama Y, Hill JL, Gettes LS. Interaction of acidosis and increased extracellular potassium on action potential characteristics and conduction in guinea pig ventricular muscle. *Circ Res* 1982;**51**:614–23.
37. Sato R, Noma A, Kurachi Y, Irisawa H. Effects of intracellular acidification on membrane currents in ventricular cells of the guinea pig. *Circ Res* 1985;**57**:553–61.
38. Irisawa H, Sato R. Intra- and extracellular actions of proton on the calcium current of isolated guinea pig ventricular cells. *Circ Res* 1986;**59**:348–55.
39. Shaw RM, Rudy Y. Electrophysiologic effects of acute myocardial ischemia: a theoretical study of altered cell excitability and action potential duration. *Cardiovasc Res* 1997;**35**:256–72.
40. Shaw RM, Rudy Y. Ionic mechanisms of propagation in cardiac tissue. Roles of the sodium and L-type calcium currents during reduced excitability and decreased gap junction coupling. *Circ Res* 1997;**81**:727–41.
41. Hund TJ, Kucera JP, Otani NF, Rudy Y. Ionic charge conservation and long-term steady state in the Luo-Rudy dynamic cell model. *Biophys J* 2001;**81**:3324–31.
42. Roberts BN, Christini DJ. NHE inhibition does not improve Na(+) or Ca(2+) overload during reperfusion: using modeling to illuminate the mechanisms underlying a therapeutic failure. *PLoS Comput Biol* 2011;**7**:e1002241.
43. Noma A. ATP-regulated K^+ channels in cardiac muscle. *Nature* 1983;**305**:147–8.
44. Ferrero JM Jr, Saiz J, Ferrero JM, Thakor NV. Simulation of action potentials from metabolically impaired cardiac myocytes. Role of ATP-sensitive K^+ current. *Circ Res* 1996;**79**:208–21.
45. Horie M, Irisawa H, Noma A. Voltage-dependent magnesium block of adenosine-triphosphate-sensitive potassium channel in guinea-pig ventricular cells. *J Physiol* 1987;**387**:251–72.
46. Trautwein W, Gottstein U, Dudel J. The action current of the myocardial fibers in oxygen deficiency. *Pflugers Arch* 1954;**260**:40–60.
47. Rodriguez B, Ferrero JM Jr, Trenor B. Mechanistic investigation of extracellular K^+ accumulation during acute myocardial ischemia: a simulation study. *Am J Physiol Heart Circ Physiol* 2002;**283**:H490–500.
48. Cook DL, Satin LS, Ashford ML, Hales CN. ATP-sensitive K^+ channels in pancreatic beta-cells. Spare-channel hypothesis. *Diabetes* 1988;**37**:495–8.
49. Yan GX, Yamada KA, Kleber AG, McHowat J, Corr PB. Dissociation between cellular K^+ loss, reduction in repolarization time, and tissue ATP levels during myocardial hypoxia and ischemia. *Circ Res* 1993;**72**:560–70.

50. Shaw RM, Rudy Y. Electrophysiologic effects of acute myocardial ischemia. A mechanistic investigation of action potential conduction and conduction failure. *Circ Res* 1997;**80**:124–38.
51. Michailova A, Saucerman J, Belik ME, McCulloch AD. Modeling regulation of cardiac KATP and L-type Ca^{2+} currents by ATP, ADP, and Mg^{2+}. *Biophys J* 2005;**88**: 2234–49.
52. Michailova A, Lorentz W, McCulloch A. Modeling transmural heterogeneity of K(ATP) current in rabbit ventricular myocytes. *Am J Physiol Cell Physiol* 2007;**293**: C542–57.
53. Downar E, Janse MJ, Durrer D. The effect of 'ischemic' blood on transmembrane potentials of normal porcine ventricular myocardium. *Circulation* 1977;**55**:455–62.
54. Harris AS, Bisteni A, Russell RA, Brigham JC, Firestone JE. Excitatory factors in ventricular tachycardia resulting from myocardial ischemia; potassium a major excitant. *Science* 1954;**119**:200–3.
55. Kleber AG. Conduction of the impulse in the ischemic myocardium—implications for malignant ventricular arrhythmias. *Experientia* 1987;**43**:1056–61.
56. Zeng J, Laurita KR, Rosenbaum DS, Rudy Y. Two components of the delayed rectifier K^+ current in ventricular myocytes of the guinea pig type. Theoretical formulation and their role in repolarization. *Circ Res* 1995;**77**:140–52.
57. Ju YK, Saint DA, Gage PW. Hypoxia increases persistent sodium current in rat ventricular myocytes. *J Physiol* 1996;**497**(Pt 2):337–47.
58. Wilde AA, Aksnes G. Myocardial potassium loss and cell depolarisation in ischaemia and hypoxia. *Cardiovasc Res* 1995;**29**:1–15.
59. Wilde AA, Peters RJ, Janse MJ. Catecholamine release and potassium accumulation in the isolated globally ischemic rabbit heart. *J Mol Cell Cardiol* 1988;**20**:887–96.
60. Shivkumar K, Deutsch NA, Lamp ST, Khuu K, Goldhaber JI, Weiss JN. Mechanism of hypoxic K loss in rabbit ventricle. *J Clin Invest* 1997;**100**:1782–8.
61. Kleber AG, Riegger CB, Janse MJ. Extracellular K^+ and H^+ shifts in early ischemia: mechanisms and relation to changes in impulse propagation. *J Mol Cell Cardiol* 1987; **19**(Suppl 5):35–44.
62. Pollard AE. From myocardial cell models to action potential propagation. *J Electrocardiol* 2003;**36**(Suppl):43–9.
63. Zaitsev AV, Guha PK, Sarmast F, Kolli A, Berenfeld O, Pertsov AM *et al.* Wavebreak formation during ventricular fibrillation in the isolated, regionally ischemic pig heart. *Circ Res* 2003;**92**:546–53.
64. Janse MJ, Cinca J, Morena H, Fiolet JW, Kleber AG, de Vries GP *et al.* The 'border zone' in myocardial ischemia. An electrophysiological, metabolic, and histochemical correlation in the pig heart. *Circ Res* 1979;**44**:576–88.
65. Walfridsson H, Odman S, Lund N. Myocardial oxygen pressure across the lateral border zone after acute coronary occlusion in the pig heart. *Adv Exp Med Biol* 1985;**191**:203–10.
66. Coronel R, Fiolet JW, Wilms-Schopman FJ, Schaapherder AF, Johnson TA, Gettes LS *et al.* Distribution of extracellular potassium and its relation to electrophysiologic changes during acute myocardial ischemia in the isolated perfused porcine heart. *Circulation* 1988;**77**:1125–38.
67. Coronel R. Heterogeneity in extracellular potassium concentration during early myocardial ischaemia and reperfusion: implications for arrhythmogenesis. *Cardiovasc Res* 1994;**28**:770–7.
68. Potse M, Coronel R, LeBlanc AR, Vinet A. The role of extracellular potassium transport in computer models of the ischemic zone. *Med Biol Eng Comput* 2007;**45**: 1187–99.
69. Niederer S. Regulation of ion gradients across myocardial ischemic border zones: a biophysical modelling analysis. *PLoS ONE* 2013;**8**:e60323.
70. Wilensky RL, Tranum-Jensen J, Coronel R, Wilde AA, Fiolet JW, Janse MJ. The subendocardial border zone during acute ischemia of the rabbit heart: an electrophysiologic, metabolic, and morphologic correlative study. *Circulation* 1986;**74**: 1137–46.
71. Ferrero JM Jr, Trenor B, Rodriguez B, Saiz J. Electrical activity and reentry during acute regional myocardial ischemia: insights from simulations. *Int J Bifurcation Chaos* 2003;**13**:3703–15.
72. Coronel R. Distribution of extracellular potassium during myocardial ischemia. *Ph.D. Thesis*. University of Amsterdam, 1988.
73. Kleber AG, Janse MJ, van Capelle FJ, Durrer D. Mechanism and time course of S-T and T-Q segment changes during acute regional myocardial ischemia in the pig heart determined by extracellular and intracellular recordings. *Circ Res* 1978;**42**: 603–13.
74. Pogwizd SM, Corr PB. Electrophysiologic mechanisms underlying arrhythmias due to reperfusion of ischemic myocardium. *Circulation* 1987;**76**:404–26.
75. Bernus O, Zemlin CW, Zaritsky RM, Mironov SF, Pertsov AM. Alternating conduction in the ischaemic border zone as precursor of reentrant arrhythmias: a simulation study. *Europace* 2005;**7**:S93–104.
76. Kimura S, Bassett AL, Gaide MS, Kozlovskis PL, Myerburg RJ. Regional changes in intracellular potassium and sodium activity after healing of experimental myocardial infarction in cats. *Circ Res* 1986;**58**:202–8.
77. Fujiwara H, Ashraf M, Sato S, Millard RW. Transmural cellular damage and blood flow distribution in early ischemia in pig hearts. *Circ Res* 1982;**51**:683–93.
78. Jie X, Rodriguez B, de Groot JR, Coronel R, Trayanova N. Reentry in survived subepicardium coupled to depolarized and inexcitable midmyocardium: insights into arrhythmogenesis in ischemia phase 1B. *Heart Rhythm* 2008;**5**:1036–44.
79. Jie X, Trayanova NA. Mechanisms for initiation of reentry in acute regional ischemia phase 1B. *Heart Rhythm* 2010;**7**:379–86.
80. Costeas C, Peters NS, Waldecker B, Ciaccio EJ, Wit AL, Coromilas J. Mechanisms causing sustained ventricular tachycardia with multiple QRS morphologies: results of mapping studies in the infarcted canine heart. *Circulation* 1997;**96**:3721–31.
81. Heidenreich E, Ferrero JM, Rodriguez JF. Modeling the human heart under acute ischemia. In: Calbo E, Peña B (eds). *Patient-Specific Computational Modeling*. Dordrecht, The Netherlands: Springer; 2012.
82. Heidenreich E. Algorithms for reaction-diffusion equations applied to electrophysiology. *Ph.D. Thesis*. University of Zaragoza, 2009.
83. de Groot JR, Coronel R. Acute ischemia-induced gap junctional uncoupling and arrhythmogenesis. *Cardiovasc Res* 2004;**62**:323–34.
84. Trenor B, Romero L, Ferrero JM Jr, Saiz J, Molto G, Alonso JM. Vulnerability to reentry in a regionally ischemic tissue: a simulation study. *Ann Biomed Eng* 2007; **35**:1756–70.
85. Fan Z, Nakayama K, Hiraoka M. Multiple actions of pinacidil on adenosine triphosphate-sensitive potassium channels in guinea-pig ventricular myocytes. *J Physiol* 1990;**430**:273–95.
86. Trenor B, Ferrero JM Jr, Rodriguez B, Montilla F. Effects of pinacidil on reentrant arrhythmias generated during acute regional ischemia: a simulation study. *Ann Biomed Eng* 2005;**33**:897–906.
87. Clarkson CW, Matsubara T, Hondeghem LM. Evidence for voltage-dependent block of cardiac sodium channels by tetrodotoxin. *J Mol Cell Cardiol* 1988;**20**: 1119–31.
88. Cardona K, Trenor B, Molto G, Martinez M, Ferrero JM Jr, Starmer F *et al.* Exploring the role of pH in modulating the effects of lidocaine in virtual ischemic tissue. *Am J Physiol Heart Circ Physiol* 2010;**299**:H1615–24.
89. Tice BM, Rodríguez B, Eason J, Trayanova N. Mechanistic investigation into the arrhythmogenic role of transmural heterogeneities in regional ischaemia phase 1A. *Europace* 2007;**9**(Suppl 6):vi46–58.
90. Weiss DL, Ifland M, Sachse FB, Seemann G, Dossel O. Modeling of cardiac ischemia in human myocytes and tissue including spatiotemporal electrophysiological variations. *Biomed Tech (Berl)* 2009;**54**:107–25.
91. Kuo CS, Reddy CP, Munakata K, Surawicz B. Arrhythmias dependent predominantly on dispersion of repolarization. In: Zipes DP, Jalife J (eds). *Cardiac Electrophysiology and Arrhythmias*. Orlando: Grune and Stratton; 1985:277–85.
92. Moe GK, Rheinboldt WC, Abildskov JA. A computer model of atrial fibrillation. *Am Heart J* 1964;**67**:200–20.
93. Clayton RH, Holden AV. Dispersion of cardiac action potential duration and the initiation of re-entry: a computational study. *Biomed Eng Online* 2005;**4**:11.
94. Romero L, Trenor B, Alonso JM, Tobon C, Saiz J, Ferrero JM Jr. The relative role of refractoriness and source-sink relationship in reentry generation during simulated acute ischemia. *Ann Biomed Eng* 2009;**37**:1560–71.
95. Delgado C, Steinhaus B, Delmar M, Chialvo DR, Jalife J. Directional differences in excitability and margin of safety for propagation in sheep ventricular epicardial muscle. *Circ Res* 1990;**67**:97–110.
96. Wang Y, Rudy Y. Action potential propagation in inhomogeneous cardiac tissue: safety factor considerations and ionic mechanism. *Am J Physiol Heart Circ Physiol* 2000;**278**:H1019–29.
97. Jie X, Gurev V, Trayanova N. Mechanisms of mechanically induced spontaneous arrhythmias in acute regional ischemia. *Circ Res* 2010;**106**:185–92.
98. Kelly D, Mackenzie L, Hunter P, Smaill B, Saint DA. Gene expression of stretch-activated channels and mechanoelectric feedback in the heart. *Clin Exp Pharmacol Physiol* 2006;**33**:642–8.
99. Craelius W. Stretch-activation of rat cardiac myocytes. *Exp Physiol* 1993;**78**: 411–23.
100. Pollard AE, Cascio WE, Fast VG, Knisley SB. Modulation of triggered activity by uncoupling in the ischemic border. A model study with phase 1b-like conditions. *Cardiovasc Res* 2002;**56**:381–92.
101. Clayton RH, Nash MP, Bradley CP, Panfilov AV, Paterson DJ, Taggart P. Experiment-model interaction for analysis of epicardial activation during human ventricular fibrillation with global myocardial ischaemia. *Prog Biophys Mol Biol* 2011;**107**:101–11.
102. Rodriguez B, Tice BM, Eason JC, Aguel F, Ferrero JM, Trayanova N. Effect of acute global ischemia on the upper limit of vulnerability: a simulation study. *Am J Physiol Heart Circ Physiol* 2004;**286**:H2078–88.
103. Rodriguez B, Tice BM, Eason JC, Aguel F, Trayanova N. Cardiac vulnerability to electric shocks during phase 1A of acute global ischemia. *Heart Rhythm* 2004;**1**: 695–703.

104. El-Sherif N, Scherlag BJ, Lazzara R, Hope RR. Re-entrant ventricular arrhythmias in the late myocardial infarction period. 1. Conduction characteristics in the infarction zone. *Circulation* 1977;**55**:686–702.
105. Lue WM, Boyden PA. Abnormal electrical properties of myocytes from chronically infarcted canine heart. Alterations in V_{max} and the transient outward current. *Circulation* 1992;**85**:1175–88.
106. Litwin SE, Bridge JH. Enhanced Na(+)-Ca^{2+} exchange in the infarcted heart. Implications for excitation-contraction coupling. *Circ Res* 1997;**81**:1083–93.
107. Gough WB, Mehra R, Restivo M, Zeiler RH, el Sherif N. Reentrant ventricular arrhythmias in the late myocardial infarction period in the dog. 13. Correlation of activation and refractory maps. *Circ Res* 1985;**57**:432–42.
108. Cabo C, Boyden PA. Electrical remodeling of the epicardial border zone in the canine infarcted heart: a computational analysis. *Am J Physiol Heart Circ Physiol* 2003;**284**:H372–84.
109. Aggarwal R, Boyden PA. Diminished Ca^{2+} and Ba^{2+} currents in myocytes surviving in the epicardial border zone of the 5-day infarcted canine heart. *Circ Res* 1995;**77**:1180–91.
110. Jiang M, Cabo C, Yao J, Boyden PA, Tseng G. Delayed rectifier K currents have reduced amplitudes and altered kinetics in myocytes from infarcted canine ventricle. *Cardiovasc Res* 2000;**48**:34–43.
111. Pinto JM, Boyden PA. Electrical remodeling in ischemia and infarction. *Cardiovasc Res* 1999;**42**:284–97.
112. Decker KF, Rudy Y. Ionic mechanisms of electrophysiological heterogeneity and conduction block in the infarct border zone. *Am J Physiol Heart Circ Physiol* 2010;**299**:H1588–97.
113. Aggarwal R, Pu J, Boyden PA. Ca(2+)-dependent outward currents in myocytes from epicardial border zone of 5-day infarcted canine heart. *Am J Physiol* 1997;**273**(Pt 2):H1386–94.
114. McDowell KS, Arevalo HJ, Maleckar MM, Trayanova NA. Susceptibility to arrhythmia in the infarcted heart depends on myofibroblast density. *Biophys J* 2011;**101**:1307–15.
115. Dillon SM, Allessie MA, Ursell PC, Wit AL. Influences of anisotropic tissue structure on reentrant circuits in the epicardial border zone of subacute canine infarcts. *Circ Res* 1988;**63**:182–206.
116. Smith JH, Green CR, Peters NS, Rothery S, Severs NJ. Altered patterns of gap junction distribution in ischemic heart disease. An immunohistochemical study of human myocardium using laser scanning confocal microscopy. *Am J Pathol* 1991;**139**:801–21.
117. Kleber AG, Rudy Y. Basic mechanisms of cardiac impulse propagation and associated arrhythmias. *Physiol Rev* 2004;**84**:431–88.
118. Rudy Y. Lessons learned about slow discontinuous conduction from models of impulse propagation. *J Electrocardiol* 2005;**38**(Suppl):52–4.
119. Wilders R, Wagner MB, Golod DA, Kumar R, Wang YG, Goolsby WN *et al.* Effects of anisotropy on the development of cardiac arrhythmias associated with focal activity. *Pflugers Arch* 2000;**441**:301–12.
120. Monserrat M, Saiz J, Ferrero JM Jr, Ferrero JM, Thakor NV. Ectopic activity in ventricular cells induced by early afterdepolarizations developed in Purkinje cells. *Ann Biomed Eng* 2000;**28**:1343–51.
121. Rohr S. Myofibroblasts in diseased hearts: new players in cardiac arrhythmias? *Heart Rhythm* 2009;**6**:848–56.
122. Porter KE, Turner NA. Cardiac fibroblasts: at the heart of myocardial remodeling. *Pharmacol Ther* 2009;**123**:255–78.
123. Gaudesius G, Miragoli M, Thomas SP, Rohr S. Coupling of cardiac electrical activity over extended distances by fibroblasts of cardiac origin. *Circ Res* 2003;**93**:421–8.
124. Miragoli M, Gaudesius G, Rohr S. Electrotonic modulation of cardiac impulse conduction by myofibroblasts. *Circ Res* 2006;**98**:801–10.
125. de Bakker JM, van Capelle FJ, Janse MJ, Tasseron S, Vermeulen JT, N de Jonge *et al.* Fractionated electrograms in dilated cardiomyopathy: origin and relation to abnormal conduction. *J Am Coll Cardiol* 1996;**27**:1071–8.
126. MacCannell KA, Bazzazi H, Chilton L, Shibukawa Y, Clark RB, Giles WR. A mathematical model of electrotonic interactions between ventricular myocytes and fibroblasts. *Biophys J* 2007;**92**:4121–32.
127. Sachse FB, Moreno AP, Abildskov JA. Electrophysiological modeling of fibroblasts and their interaction with myocytes. *Ann Biomed Eng* 2008;**36**:41–56.
128. Maleckar MM, Greenstein JL, Giles WR, Trayanova NA. Electrotonic coupling between human atrial myocytes and fibroblasts alters myocyte excitability and repolarization. *Biophys J* 2009;**97**:2179–90.
129. Xie Y, Garfinkel A, Camelliti P, Kohl P, Weiss JN, Qu Z. Effects of fibroblast-myocyte coupling on cardiac conduction and vulnerability to reentry: a computational study. *Heart Rhythm* 2009;**6**:1641–9.
130. Jacquemet V, Henriquez CS. Loading effect of fibroblast-myocyte coupling on resting potential, impulse propagation, and repolarization: insights from a microstructure model. *Am J Physiol Heart Circ Physiol* 2008;**294**:H2040–52.
131. Jacquemet V, Henriquez CS. Genesis of complex fractionated atrial electrograms in zones of slow conduction: a computer model of microfibrosis. *Heart Rhythm* 2009;**6**:803–10.
132. Petrov VS, Osipov GV, Kurths J. Fibroblasts alter spiral wave stability. *Chaos* 2010;**20**:045103.
133. Engelman ZJ, Trew ML, Smaill BH. Structural heterogeneity alone is a sufficient substrate for dynamic instability and altered restitution. *Circ Arrhythm Electrophysiol* 2010;**3**:195–203.
134. Turner I, Huang H, Saumarez RC. Numerical simulation of paced electrogram fractionation: relating clinical observations to changes in fibrosis and action potential duration. *J Cardiovasc Electrophysiol* 2005;**16**:151–61.
135. Vadakkumpadan F, Arevalo H, Prassl AJ, Chen J, Kickinger F, Kohl P *et al.* Image-based models of cardiac structure in health and disease. *Interdiscip Rev Syst Biol Med* 2010;**2**:489–506.
136. Rantner LJ, Arevalo HJ, Constantino JL, Efimov IR, Plank G, Trayanova NA. Three-dimensional mechanisms of increased vulnerability to electric shocks in myocardial infarction: altered virtual electrode polarizations and conduction delay in the peri-infarct zone. *J Physiol* 2012;**590**(Pt 18):4537–51.
137. Vigmond E, Vadakkumpadan F, Gurev V, Arevalo H, Deo M, Plank G *et al.* Towards predictive modelling of the electrophysiology of the heart. *Exp Physiol* 2009;**94**:563–77.
138. Pop M, Sermesant M, Mansi T, Crystal E, Ghate S, Peyrat JM *et al.* Correspondence between simple 3-D MRI-based computer models and in-vivo EP measurements in swine with chronic infarctions. *IEEE Trans Biomed Eng* 2011;**58**:3483–6.
139. Pop M, Sermesant M, Liu G, Relan J, Mansi T, Soong A *et al.* Construction of 3D MR image-based computer models of pathologic hearts, augmented with histology and optical fluorescence imaging to characterize action potential propagation. *Med Image Anal* 2012;**16**:505–23.
140. Ng J, Jacobson JT, Ng JK, Gordon D, Lee DC, Carr JC *et al.* Virtual electrophysiological study in a 3-dimensional cardiac magnetic resonance imaging model of porcine myocardial infarction. *J Am Coll Cardiol* 2012;**60**:423–30.
141. Ashikaga H, Arevalo H, Vadakkumpadan F, Blake RC III, Bayer JD, Nazarian S *et al.* Feasibility of image-based simulation to estimate ablation target in human ventricular arrhythmia. *Heart Rhythm* 2013;**10**:1109–16 .